Force Transmission between Three Tissues Controls Bipolar Planar Polarity Establishment and Morphogenesis

Ghislain Gillard, Ophélie Nicolle, Thibault Brugière, Sylvain Prigent, Mathieu Pinot, Grégoire Michaux

HAL Id: hal-02119227

https://univ-rennes.hal.science/hal-02119227

Submitted on 18 Jul 2019

Force transmission between three tissues controls bipolar planar polarity establishment and morphogenesis

Ghislain Gillard[1,†], Ophélie Nicolle[1], Thibault Brugière[1], Sylvain Prigent[2], Mathieu Pinot[1], Grégoire Michaux[1,*]

[1] CNRS, Univ Rennes, IGDR (Institut de Génétique et Développement de Rennes) - UMR6290, 2 avenue du Professeur Léon Bernard, F-35000 Rennes, France

[2] Biogenouest, Bio-imaging axis, 16 Le Clos, F-35590 Saint-Gilles, France; Univ Rennes, Microscopy Rennes Imaging Center, Biosit - UMS CNRS 3480/US INSERM 018, 2 avenue du Professeur Léon Bernard, F-35000 Rennes, France.

[†] Current address: MRC LMB, Cambridge, UK.

[*] Lead contact and corresponding author: Grégoire Michaux; gmichaux@univ-rennes1.fr

Summary

How tissues from different developmental origins interact to achieve coordinated morphogenesis at the level of a whole organism is a fundamental question in developmental biology. While biochemical signalling pathways controlling morphogenesis have been extensively studied [1-3], morphogenesis of epithelial tissues can also be directed by mechanotransduction pathways physically linking two tissues [4-8]. *C. elegans* embryonic elongation requires the coordination of three tissues: muscles, the dorsal and ventral epidermis and the lateral epidermis. Elongation starts by cell shape changes driven by actomyosin contractions in the lateral epidermis [9, 10]. At mid-elongation muscles become connected to the apical surface of the dorsal and ventral epidermis by molecular tendons formed by muscle integrins, extracellular matrix and *C. elegans* hemidesmosomes (CeHDs). The mechanical signal generated by the onset of muscle contractions in the antero-posterior axis from mid-elongation is translated into a biochemical pathway controlling the maturation of CeHDs in the dorsal and ventral epidermis [11]. Consistently mutations affecting muscle contractions or molecular tendons lead to a mid-elongation arrest [12]. Here we found that the mechanical force generated by muscle contractions and relayed by molecular tendons is transmitted by adherens junctions to lateral epidermal cells where it establishes a newly identified bipolar planar polarity of the apical PAR module. The planar polarised PAR module is then required for actin planar organisation, thus contributing to determine the orientation of cell shape changes and the elongation axis of the whole embryo. This mechanotransduction pathway is therefore essential to coordinate the morphogenesis of three embryonic tissues.

Results and discussion

At the beginning of *C. elegans* embryonic elongation the long axis of lateral epidermal cells is oriented along the dorso-ventral (D/V) axis. Actomyosin contractions in these cells progressively reduce cell length along the D/V axis and increase it along the antero-posterior (A/P) axis, inducing a 90° shift of the cell long axis from the D/V to the A/P axis. This process takes place in the plane of the apical membrane (Figure S1A-B). This orientation shift becomes obvious at the 2-fold stage and is concomitant with a progressive planar organisation of actin fibres along the D/V axis in the lateral epidermis. While actin is partially disorganised at the 1.5-fold stage (Figure S1E-E') it becomes mostly oriented along the D/V axis from the 2-fold stage (Figure S1F-G') as was recently shown [13]. To identify the mechanisms underlying actin planar polarisation we looked for planar polarised factors in lateral epidermal cells. Previous studies have only identified a few which are not required for embryonic elongation [14-16] while canonical planar cell polarity (PCP) is mostly required in neurons but not during elongation [17, 18]. During *Drosophila* embryonic morphogenesis Bazooka/Par-3 becomes planar polarised in a bipolar manner [19]. Using CRISPR/Cas9 genome edited strains to localise endogenous PAR-3::GFP, PAR-6::GFP and GFP::PKC-3 [20], we found that they exhibit bipolar planar polarity in lateral cells during elongation, accumulating on junctions between lateral cells (L-L junctions) but not on junction between lateral and ventral or dorsal cells (L-D/V junctions) (Figure 1A-D, E-E', H-H'); a similar localisation was observed with a PAR-3::GFP line generated independently [21] (Figure S2H). We found that the PAR proteins progressively disappear from the L-D/V junctions between the 1.5- and the 2-fold stage (Figures 1A-D; S2A-C"), while actin becomes oriented along the D/V axis (Figure S1E-G'). To test the role of apical PAR module components in their mutual planar localisation we showed that PAR-3 is essential for PAR-6 and PKC-3

recruitment at L-L junctions (Figure 1E-J), while PAR-6 enables the recruitment of PAR-3 (Figure S2D-F).

Because we never observed PAR proteins recruitment on the junctions between ventral or dorsal cells (Figure 1B, E, H blue arrows) we hypothesized that they have a specific function on L-L junctions in lateral cells. Genetic tools have already been used to analyse the role of PAR-3 and PAR-6 in epidermal cells during early elongation; however the embryos arrested before the 2-fold stage [21, 22] precluding the analysis of their role in actin organisation at later stages. We therefore depleted PAR-3 by RNAi using conditions leading to a 2-fold arrest (see STAR Methods). In these embryos we observed that actin could be either disorganised or oriented in the A/P axis (Figure 1K-M). Most strikingly some cells were elongated in the D/V axis (Figure 1L) and systematically displayed A/P oriented actin (19/19 D/V elongated cells; Figure S3M), strongly suggesting a correlation between orientation of actin filaments and the cell long axis. We concluded that the PAR module is planar polarised and that PAR-3 is required for actin planar reorganisation in lateral epidermal cells.

Despite the absence of a direct connection between muscles and the lateral epidermis (Figure S1C) there is a tight correlation in time between the onset of muscle contractions and the establishment of planar polarity from the 1.5-fold stage onwards. Moreover mutations affecting muscle contractions or components of molecular tendons trigger a 2-fold elongation arrest and were shown to induce an elongation of lateral cells in the D/V axis [23] as observed following PAR-3 depletion (Figure 1L). To examine the role of muscle contractions in actin organisation we first targeted genes expressed only in muscles (Figure S1D): *unc-112/*kindlin is essential for myosin heavy chain organisation in myofilaments and PAT-3/β-integrin localisation [24, 25] whereas the *pat-4*/ILK interacts with integrin adhesion complexes [26].

4

Depletion of these genes disrupted the elongation axis of some cells (Figure 2C, cell V1) and the planar polarity of actin in lateral epidermal cells (Figure 2A-C'), suggesting that muscle contractions induce a mechanical signal transmitted to the lateral epidermis. We next investigated the function of CeHDs by depleting two genes expressed in the dorsal and ventral epidermis: *unc-52* encodes an extracellular matrix (ECM) perlecan secreted basolaterally [27] and *vab-10* is a spectraplakin homologue and a structural protein of CeHDs [28]. We found that these genes are also required for the elongation axis of some cells (Figure 2E, cell V3) and the planar polarity of actin in lateral epidermal cells (Figure 2D-E'). We thus concluded that a biomechanical signal initiated by muscle contractions is relayed by molecular tendons in the dorsal and ventral epidermis and is required for actin organisation in lateral epidermal cells.

We next addressed the functional relationship between muscle contractions and PAR proteins planar localisation. We found that *unc-112*, *pat-4*, *unc-52*, and *vab-10* are all required for the bipolar planar polarised localisation of PAR-3 (Figure 2F-K). To determine whether muscle contractions are required for the establishment or the maintenance of planar polarity we quantified PAR-3 recruitment during elongation. In control embryos PAR-3 is first localised in a junction-like manner at the apical side of lateral cells; planar polarity is then established from the 1.5-fold stage and peaks between the 2- and the 3-fold stage (Figure 1D). We abolished muscle contractions using an *unc-112(RNAi)* background and found that PAR-3 was weakly planar polarised both in control and *unc-112(RNAi)* embryos before the 1.5-fold stage while *unc-112* becomes required to maintain PAR-3 localisation on L-L junctions from the 1.5 fold stage (Figures 2L; S2G). This observation demonstrates that the biomechanical signal emitted by muscle contractions is not necessary for the initial PAR-3 plasma membrane recruitment but is required for the establishment of its robust bipolar planar polarity. Finally

we established that *unc-112* is also required for the planar polarity of PAR-6 and PKC-3 (Figure 2M-R). We concluded that the planar polarised localisation of the PAR module is controlled by a biomechanical signal initiated by muscle contractions and relayed by molecular tendons. The PAR module is then needed to properly orient actin in the D/V axis in the lateral epidermis. In line with the absence of the PAR module at the junctions between ventral or dorsal cells, orientation of actin cables in these cells do not require this pathway (Figures 1L; 2A-E blue arrows).

In a subsequent RNAi screen designed to find new genes required for actin and PAR-3 planar polarity (Table S1) we identified the small GTPase RAB-1. RAB-1 depletion by RNAi induces a paralysed 2-fold arrest (Figure S3A-B) and actin disorganisation (Figure 3A-C). We observed a frequent 90° shift in actin organisation in the A/P axis (Figure 3B-C); this phenotype was more frequent than in *par-3(RNAi)* embryos and associated with cell axis elongation in the D/V rather than the A/P axis (Figures 3C; S3M). To evaluate the links between actin organisation and cell elongation we plotted lateral cell eccentricity and actin organisation. We found that in control and *rab-1(RNAi)* embryos there is a close correlation between actin organisation in parallel filaments and robust cell eccentricity (Figure 3D) confirming a link between actin organisation and cell elongation. We also found that *rab-1* depletion triggers a loss of PAR-3, PAR-6 and PKC-3 accumulation at L-L junctions (Figures 3E-G; S3C-H). In yeast and mammalian cells Rab1 regulates early secretion [29, 30], suggesting that it could be required for the secretion of molecular tendons components. We therefore examined the localisation of the basolateral transmembrane receptor LET-805/myotactin and of the UNC-52/perlecan, both secreted by dorsal and ventral cells. We found that *rab-1* depletion leads to a disruption of UNC-52 and LET-805 localisation (Figure 3H-K). To confirm that the whole molecular tendon structure was affected we showed that

rab-1 depletion also disrupts UNC-112 and PAT-3/β-integrin localisation in muscles (Figure S3I-L). Our results therefore suggest that RAB-1 has a function in regulating CeHDs formation presumably by controlling the secretion of at least some CeHDs essential components; however we cannot rule out a similar function in muscles where it could also be required for PAT-3 secretion. The simultaneous loss of several molecular tendon components could explain the more severe actin phenotype observed in *rab-1(RNAi)* (Figure 3C) compared to the depletion of individual components (Figure 2A-E) although we cannot exclude other functions for RAB-1 in the regulation of planar polarity.

We found that UNC-112, PAT-4, UNC-52, VAB-10 and RAB-1 control the onset and the transduction of the biomechanical signal generated by muscles leading to planar polarity establishment in lateral cells. However the loss of PAR proteins and actin planar polarity could be explained by a global loss of epithelial polarity of lateral epidermal cells. We therefore examined junction integrity and apico-basal polarity using *unc-112(RNAi)* or *rab-1(RNAi)* to abolish muscle contractions or signal transduction respectively. A combination of *in vivo* localisation, fluorescence recovery after photo-bleaching (FRAP) experiments and transmission electron microscopy (TEM) studies established that adherens junctions (AJs) are not affected (Figure 4A-C; Figure S4A-M). We observed a slight decrease of E-cadherin membrane accumulation in *rab-1(RNAi)* (Figure 4D) but not *unc-112(RNAi)* embryos (Figure S4H), consistently with a role of RAB-1 in E-cadherin secretion. To further test the integrity of apico-basal polarity we established that the apical transmembrane protein CHE-14 [31, 32] and the basolateral polarity determinant LET-413/Scribble [33] were also normally localised (Figure S4N-Q). Altogether these results demonstrate that muscle biomechanical signalling is not required to establish or maintain junction integrity and apico-basal polarity in lateral epidermal cells.

We next sought to identify the possible signal transduction mechanism between the dorsal and ventral epidermis and the lateral epidermis. Given the biomechanical nature of the signal we hypothesised that the putative transduction pathway could also be mechanical. For example the apical extracellular matrix (aECM) might relay the deformations observed in dorsal and ventral cells upon muscle contractions [11] ; however depletion of aECM components triggers later elongation arrest and embryo bursting [34, 35] which are not consistent with our observations. AJs could also relay the biomechanical signal generated by muscles between the dorsal or ventral epidermis and the lateral epidermis. To test this possibility we depleted HMP-1/α-catenin to induce a 2-fold stage arrest and block a putative cell-cell signalling based on the E-cadherin/catenins complex. We found that PAR-3 failed to be recruited to L-L junctions in *hmp-1(RNAi)* 2-fold arrested embryos (Figure 4E-G). We therefore propose that the mechanical signal is transmitted to the lateral epidermis by AJs, although we cannot exclude that other mechanisms could also be implicated in this latter signal transduction step.

We finally assessed the consequences of actin disorganisation on tension orientation in the lateral epidermis, which might explain the 90° shift observed in the elongation axis of some lateral cells. Using laser nano-ablation we first showed that in control 2-fold stage embryos where actin is oriented in the D/V axis, a cut in the A/P axis leads to a systematic relaxation of the actin cytoskeleton, whereas a cut along the D/V axis does not lead to relaxation (Figure 4H-I, L). These results reveal that tension forces are oriented along the D/V axis in the lateral epidermis at the 2-fold stage. We then exploited a phenotype frequently observed in *rab-1(RNAi)* embryos where actin is aligned along the A/P axis instead of the D/V axis. In *rab-1* depleted embryos displaying A/P oriented actin we observed a relaxation following a D/V cut suggesting a 90° shift of tension orientation (Figure 4K-L). Surprisingly the A/P cut led to a

8

closure (Figure 4J, L) which could be explained by pushing forces exerted by the dorsal and ventral cells on the lateral epidermis; such a force would not be exerted by lateral cells, explaining why the reciprocal experiment in control embryos did not lead to a similar closure (Figure 4I, L). These results, together with the correlation between the cell elongation axis and actin organisation (Figure 3D), strongly support the hypothesis that actin orientation is the primary cause of the cell elongation axis which is itself the main cause of the embryonic elongation axis. We therefore propose that the disorganisation of actin in lateral cells observed upon disruption of the mechanical signal initiated by muscles induces the arrest at the 2-fold stage.

We found that muscle contractions initiate a mechanical signal transmitted to the lateral epidermis through dorsal and ventral molecular tendons and AJs; this signal is essential to promote a planar organisation of the PAR module and actin, thus regulating tension orientation in lateral cells. We have therefore identified a trans-tissular mechanotransduction signalling pathway required to coordinate morphogenesis between three tissues: muscles, the dorsal and ventral epidermis and the lateral epidermis during *C. elegans* embryonic morphogenesis (Figure S4R). Interestingly the mechanical signal generated by muscles is therefore at the origin of at least two different outcomes: maturation of CeHDs [11] and establishment of planar polarity in lateral cells. This pathway is very different from the canonical Wnt/PCP, Fat/Dachsous and Toll receptor pathways which enable cells to establish vectorial/unipolar planar polarity [36, 37]. However many other proteins have been found to be planar polarised in a bipolar manner, e.g. E-cadherin [38], myosin [19] and PAR-3 [19, 39] in *Drosophila* , or tropomodulin [14], microtubules and NOCA-1 [15, 16] and the apical PAR module (this study) in *C. elegans*. Interestingly there is a parallel between the mutual exclusion of PAR-3 and myosin in *Drosophila* [19, 40] and the apical PAR module and actin

9

in *C. elegans* (this study), even if myosin is not polarised in lateral cells [13]. While in *Drosophila* Rho kinase is required for PAR-3 planar polarity [41], the mechanism leading to the PAR module planar polarisation is not yet identified in *C. elegans*. For instance the often PAR associated CDC-42 GTPase has been proposed to play a role during early elongation but its function was not investigated during later elongation [42]. Future work investigating the pathway(s) leading to the PAR module bipolar planar polarity downstream of AJs, and how PAR proteins could control actin organisation in lateral cells, will be necessary to fully characterise this new mechanotransduction pathway.

Tissue mechanics and force transmission have been previously shown to be involved in *Drosophila* wing morphogenesis, where the wing hinge retraction enables planar rearrangement from a radial to a proximal-distal-oriented polarity in the wing blade [5]; similarly a mechanical input has been implicated in setting up planar polarity during *Drosophila* germ-band extension [4, 8, 41]. In a different context a recent study demonstrated that a physical pressure exerted by proliferating dermal cells controls the patterning of the avian skin [43]. However in all these examples the tissue-wide tension is generated in direct connection with the target tissue. Our results show a more complex signal transduction pathway where the tension generated by muscles is relayed along two tissues, first in the inside to outside orientation through molecular tendons, then in the D/V axis through AJs. Interestingly smooth muscles lie below or inside many tissues such as the skin, the intestine, the respiratory organs or the reproductive tracts where they could be essential for planar polarity establishment in surrounding epithelial tissues throughout the animal kingdom. We therefore believe that this new signalling pathway implicated in force transmission through several tissues could be conserved in other organisms.

Acknowledgements

Author contributions

G.G. and G.M. designed the experiments. G.G., O.N., T.B. and G.M. performed experiments and data analysis. S.P. and M.P. helped to perform quantifications and design laser nano-ablation experiments. G.G. and G.M. wrote the manuscript. GM supervised the study.

Declaration of interests

The authors declare no competing interests.

References list

1. Hubaud, A., and Pourquie, O. (2014). Signalling dynamics in vertebrate segmentation. Nature reviews. Molecular cell biology *15*, 709-721.

2. Petit, F., Sears, K.E., and Ahituv, N. (2017). Limb development: a paradigm of gene regulation. Nat Rev Genet.

3. Schmid, T., and Hajnal, A. (2015). Signal transduction during C. elegans vulval development: a NeverEnding story. Current opinion in genetics & development *32*, 1-9.

4. Collinet, C., Rauzi, M., Lenne, P.F., and Lecuit, T. (2015). Local and tissue-scale forces drive oriented junction growth during tissue extension. Nature cell biology *17*, 1247-1258.

5. Aigouy, B., Farhadifar, R., Staple, D.B., Sagner, A., Roper, J.C., Julicher, F., and Eaton, S. (2010). Cell flow reorients the axis of planar polarity in the wing epithelium of Drosophila. Cell *142*, 773-786.

6. Olguin, P., Glavic, A., and Mlodzik, M. (2011). Intertissue mechanical stress affects Frizzled-mediated planar cell polarity in the Drosophila notum epidermis. Current biology : CB *21*, 236-242.

7. Sagner, A., Merkel, M., Aigouy, B., Gaebel, J., Brankatschk, M., Julicher, F., and Eaton, S. (2012). Establishment of global patterns of planar polarity during growth of the Drosophila wing epithelium. Current biology : CB *22*, 1296-1301.

8. Butler, L.C., Blanchard, G.B., Kabla, A.J., Lawrence, N.J., Welchman, D.P., Mahadevan, L., Adams, R.J., and Sanson, B. (2009). Cell shape changes indicate a role for extrinsic tensile forces in Drosophila germ-band extension. Nature cell biology *11*, 859-864.

9. Diogon, M., Wissler, F., Quintin, S., Nagamatsu, Y., Sookhareea, S., Landmann, F., Hutter, H., Vitale, N., and Labouesse, M. (2007). The RhoGAP RGA-2 and LET-502/ROCK achieve a balance of actomyosin-dependent forces in C. elegans epidermis to control morphogenesis. Development *134*, 2469-2479.

10. Piekny, A.J., Johnson, J.L., Cham, G.D., and Mains, P.E. (2003). The Caenorhabditis elegans nonmuscle myosin genes nmy-1 and nmy-2 function as redundant components of the let-502/Rho-binding kinase and mel-11/myosin phosphatase pathway during embryonic morphogenesis. Development *130*, 5695-5704.

11. Zhang, H., Landmann, F., Zahreddine, H., Rodriguez, D., Koch, M., and Labouesse, M. (2011). A tension-induced mechanotransduction pathway promotes epithelial morphogenesis. Nature *471*, 99-103.

12. Vuong-Brender, T.T., Yang, X., and Labouesse, M. (2016). C. elegans Embryonic Morphogenesis. Curr Top Dev Biol *116*, 597-616.

13. Vuong-Brender, T.T., Ben Amar, M., Pontabry, J., and Labouesse, M. (2017). The interplay of stiffness and force anisotropies drives embryo elongation. Elife *6*.

14. Cox-Paulson, E.A., Walck-Shannon, E., Lynch, A.M., Yamashiro, S., Zaidel-Bar, R., Eno, C.C., Ono, S., and Hardin, J. (2012). Tropomodulin protects alpha-catenin-dependent junctional-actin networks under stress during epithelial morphogenesis. Current biology : CB *22*, 1500-1505.

15. Quintin, S., Wang, S., Pontabry, J., Bender, A., Robin, F., Hyenne, V., Landmann, F., Gally, C., Oegema, K., and Labouesse, M. (2016). Non-centrosomal epidermal microtubules act in parallel to LET-502/ROCK to promote C. elegans elongation. Development *143*, 160-173.

16. Wang, S., Wu, D., Quintin, S., Green, R.A., Cheerambathur, D.K., Ochoa, S.D., Desai, A., and Oegema, K. (2015). NOCA-1 functions with gamma-tubulin and in parallel to Patronin to assemble non-centrosomal microtubule arrays in C. elegans. Elife *4*, e08649.

17. Chen, C.H., He, C.W., Liao, C.P., and Pan, C.L. (2017). A Wnt-planar polarity pathway instructs neurite branching by restricting F-actin assembly through endosomal signaling. PLoS Genet *13*, e1006720.

18. Shah, P.K., Tanner, M.R., Kovacevic, I., Rankin, A., Marshall, T.E., Noblett, N., Tran, N.N., Roenspies, T., Hung, J., Chen, Z., et al. (2017). PCP and SAX-3/Robo Pathways Cooperate to

Regulate Convergent Extension-Based Nerve Cord Assembly in C. elegans. Developmental cell *41*, 195-203 e193.

19. Zallen, J.A., and Wieschaus, E. (2004). Patterned gene expression directs bipolar planar polarity in Drosophila. Developmental cell *6*, 343-355.

20. Rodriguez, J., Peglion, F., Martin, J., Hubatsch, L., Reich, J., Hirani, N., Gubieda, A.G., Roffey, J., Fernandes, A.R., St Johnston, D., et al. (2017). aPKC Cycles between Functionally Distinct PAR Protein Assemblies to Drive Cell Polarity. Developmental cell *42*, 400-415 e409.

21. Achilleos, A., Wehman, A.M., and Nance, J. (2010). PAR-3 mediates the initial clustering and apical localization of junction and polarity proteins during C. elegans intestinal epithelial cell polarization. Development *137*, 1833-1842.

22. Totong, R., Achilleos, A., and Nance, J. (2007). PAR-6 is required for junction formation but not apicobasal polarization in C. elegans embryonic epithelial cells. Development *134*, 1259-1268.

23. Hresko, M.C., Williams, B.D., and Waterston, R.H. (1994). Assembly of body wall muscle and muscle cell attachment structures in Caenorhabditis elegans. The Journal of cell biology *124*, 491-506.

24. Rogalski, T.M., Mullen, G.P., Gilbert, M.M., Williams, B.D., and Moerman, D.G. (2000). The UNC-112 gene in Caenorhabditis elegans encodes a novel component of cell-matrix adhesion structures required for integrin localization in the muscle cell membrane. The Journal of cell biology *150*, 253-264.

25. Williams, B.D., and Waterston, R.H. (1994). Genes critical for muscle development and function in Caenorhabditis elegans identified through lethal mutations. The Journal of cell biology *124*, 475-490.

26. Mackinnon, A.C., Qadota, H., Norman, K.R., Moerman, D.G., and Williams, B.D. (2002). C. elegans PAT-4/ILK functions as an adaptor protein within integrin adhesion complexes. Current biology : CB *12*, 787-797.

27. Rogalski, T.M., Williams, B.D., Mullen, G.P., and Moerman, D.G. (1993). Products of the unc-52 gene in Caenorhabditis elegans are homologous to the core protein of the mammalian basement membrane heparan sulfate proteoglycan. Genes & development *7*, 1471-1484.

28. Bosher, J.M., Hahn, B.S., Legouis, R., Sookhareea, S., Weimer, R.M., Gansmuller, A., Chisholm, A.D., Rose, A.M., Bessereau, J.L., and Labouesse, M. (2003). The Caenorhabditis elegans vab-10 spectraplakin isoforms protect the epidermis against internal and external forces. The Journal of cell biology *161*, 757-768.

29. Plutner, H., Cox, A.D., Pind, S., Khosravi-Far, R., Bourne, J.R., Schwaninger, R., Der, C.J., and Balch, W.E. (1991). Rab1b regulates vesicular transport between the endoplasmic reticulum and successive Golgi compartments. The Journal of cell biology *115*, 31-43.

30. Segev, N., Mulholland, J., and Botstein, D. (1988). The yeast GTP-binding YPT1 protein and a mammalian counterpart are associated with the secretion machinery. Cell *52*, 915-924.

31. Gillard, G., Shafaq-Zadah, M., Nicolle, O., Damaj, R., Pecreaux, J., and Michaux, G. (2015). Control of E-cadherin apical localisation and morphogenesis by a SOAP-1/AP-1/clathrin pathway in C. elegans epidermal cells. Development *142*, 1684-1694.

32. Michaux, G., Gansmuller, A., Hindelang, C., and Labouesse, M. (2000). CHE-14, a protein with a sterol-sensing domain, is required for apical sorting in C. elegans ectodermal epithelial cells. Current biology : CB *10*, 1098-1107.

33. Legouis, R., Gansmuller, A., Sookhareea, S., Bosher, J.M., Baillie, D.L., and Labouesse, M. (2000). LET-413 is a basolateral protein required for the assembly of adherens junctions in Caenorhabditis elegans. Nature cell biology *2*, 415-422.

34. Mancuso, V.P., Parry, J.M., Storer, L., Poggioli, C., Nguyen, K.C., Hall, D.H., and Sundaram, M.V. (2012). Extracellular leucine-rich repeat proteins are required to organize the apical extracellular matrix and maintain epithelial junction integrity in C. elegans. Development *139*, 979-990.

35.   Vuong-Brender, T.T.K., Suman, S.K., and Labouesse, M. (2017). The apical ECM preserves embryonic integrity and distributes mechanical stress during morphogenesis. Development *144*, 4336-4349.

36.   Aw, W.Y., and Devenport, D. (2017). Planar cell polarity: global inputs establishing cellular asymmetry. Current opinion in cell biology *44*, 110-116.

37.   Butler, M.T., and Wallingford, J.B. (2017). Planar cell polarity in development and disease. Nature reviews. Molecular cell biology *18*, 375-388.

38.   Levayer, R., Pelissier-Monier, A., and Lecuit, T. (2011). Spatial regulation of Dia and Myosin-II by RhoGEF2 controls initiation of E-cadherin endocytosis during epithelial morphogenesis. Nature cell biology *13*, 529-540.

39.   Besson, C., Bernard, F., Corson, F., Rouault, H., Reynaud, E., Keder, A., Mazouni, K., and Schweisguth, F. (2015). Planar Cell Polarity Breaks the Symmetry of PAR Protein Distribution prior to Mitosis in Drosophila Sensory Organ Precursor Cells. Current biology : CB *25*, 1104-1110.

40.   Fernandez-Gonzalez, R., Simoes Sde, M., Roper, J.C., Eaton, S., and Zallen, J.A. (2009). Myosin II dynamics are regulated by tension in intercalating cells. Developmental cell *17*, 736-743.

41.   Simoes Sde, M., Blankenship, J.T., Weitz, O., Farrell, D.L., Tamada, M., Fernandez-Gonzalez, R., and Zallen, J.A. (2010). Rho-kinase directs Bazooka/Par-3 planar polarity during Drosophila axis elongation. Developmental cell *19*, 377-388.

42.   Zilberman, Y., Abrams, J., Anderson, D.C., and Nance, J. (2017). Cdc42 regulates junctional actin but not cell polarization in the Caenorhabditis elegans epidermis. The Journal of cell biology *216*, 3729-3744.

43.   Shyer, A.E., Rodrigues, A.R., Schroeder, G.G., Kassianidou, E., Kumar, S., and Harland, R.M. (2017). Emergent cellular self-organization and mechanosensation initiate follicle pattern in the avian skin. Science *357*, 811-815.

44.   Brenner, S. (1974). The genetics of Caenorhabditis elegans. Genetics *77*, 71-94.

45.   Bouvrais, H., Chesneau, L., Pastezeur, S., Fairbrass, D., Delattre, M., and Pecreaux, J. (2018). Microtubule Feedback and LET-99-Dependent Control of Pulling Forces Ensure Robust Spindle Position. Biophys J *115*, 2189-2205.

46.   Fire, A., Xu, S., Montgomery, M.K., Kostas, S.A., Driver, S.E., and Mello, C.C. (1998). Potent and specific genetic interference by double-stranded RNA in Caenorhabditis elegans. Nature *391*, 806-811.

47.   Kamath, R.S., and Ahringer, J. (2003). Genome-wide RNAi screening in Caenorhabditis elegans. Methods *30*, 313-321.

48.   Shafaq-Zadah, M., Brocard, L., Solari, F., and Michaux, G. (2012). AP-1 is required for the maintenance of apico-basal polarity in the C. elegans intestine. Development *139*, 2061-2070.

49.   Leung, B., Hermann, G.J., and Priess, J.R. (1999). Organogenesis of the Caenorhabditis elegans intestine. Developmental biology *216*, 114-134.

50.   Cetera, M., Ramirez-San Juan, G.R., Oakes, P.W., Lewellyn, L., Fairchild, M.J., Tanentzapf, G., Gardel, M.L., and Horne-Badovinac, S. (2014). Epithelial rotation promotes the global alignment of contractile actin bundles during Drosophila egg chamber elongation. Nat Commun *5*, 5511.

51.   Gomez, J.M., Chumakova, L., Bulgakova, N.A., and Brown, N.H. (2016). Microtubule organization is determined by the shape of epithelial cells. Nat Commun *7*, 13172.
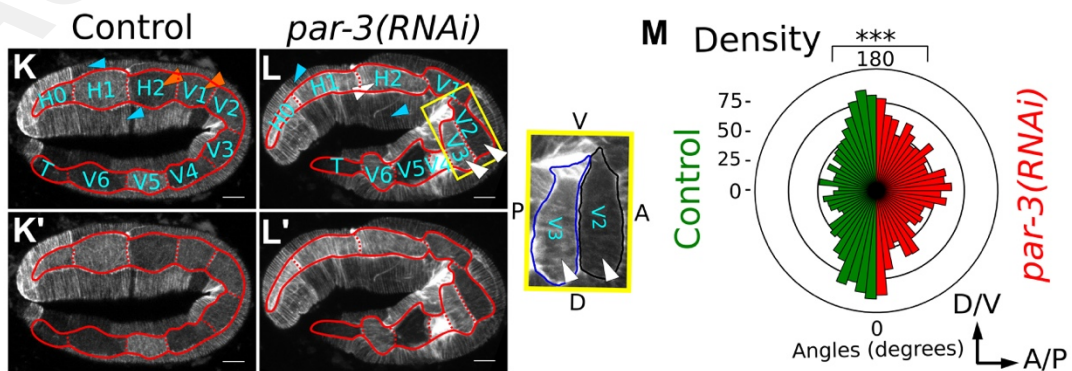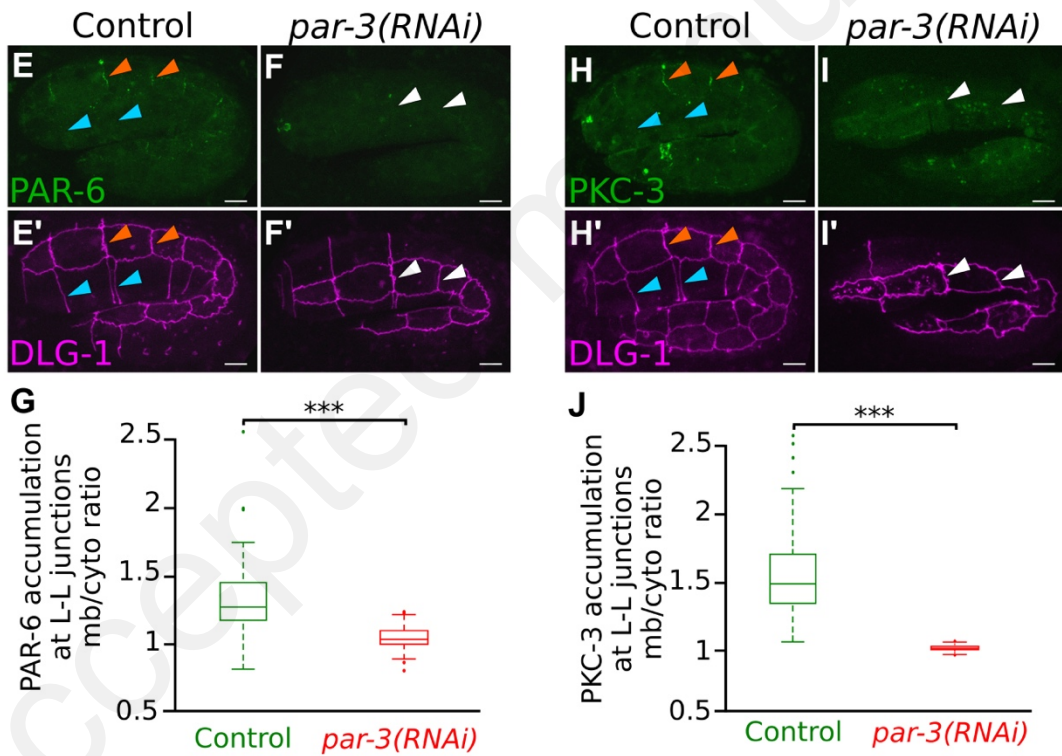
1.5-fold   **2-fold**   **3-fold**

A PAR-3   B   C

A' DLG-1   B'   C'

A"   B"   C"

mb/cyto ratio

***   ***   ***

L-L   L-D/V   L-L   L-D/V   L-L   L-D/V

PAR-3 accumulation at L-L or L-D/V junctions

D

Ratio L-L/L-DV

1.5-fold   2-fold   3-fold

PAR-3 accumulation at plasma membrane

Control   *par-3(RNAi)*   **Control**   *par-3(RNAi)*

E PAR-6   F   H PKC-3   I

E' DLG-1   F'   H' DLG-1   I'

G   PAR-6 accumulation at L-L junctions mb/cyto ratio

***

Control   *par-3(RNAi)*

J   PKC-3 accumulation at L-L junctions mb/cyto ratio

***

Control   *par-3(RNAi)*

Control   *par-3(RNAi)*

K   L

K'   L'

M   Density

180

Control   *par-3(RNAi)*

75-
50-
25-
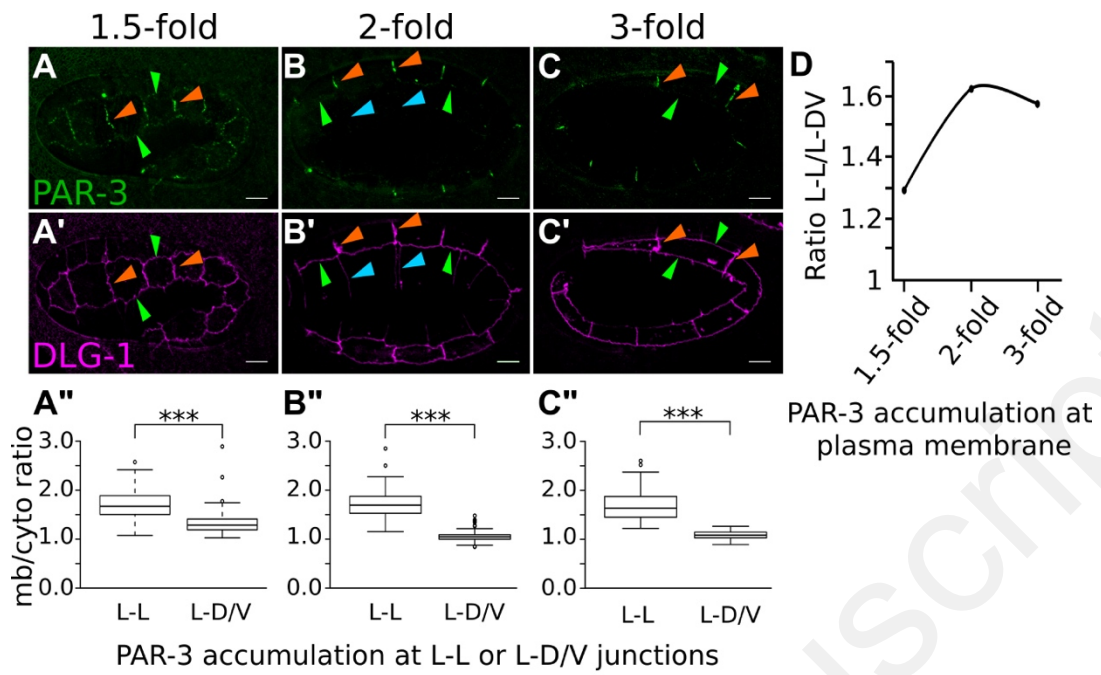
0

D/V

Angles (degrees)   A/P

17

Figure 1: The PAR module is planar polarised in the lateral epidermis and is required for actin planar polarity. A-J Observation of *C. elegans* embryos expressing endogenous PAR proteins in the epidermis at the level of the apical membrane during elongation**.** Orange arrowheads indicate L-L junctions; blue arrowheads indicate junctions between ventral cells; white arrowheads indicate absence of PAR proteins localisation at L-L junctions **A-D** Endogenous PAR-3::GFP accumulates at L-L junctions (orange arrowheads) during elongation but is not visible at junctions between ventral cells (blue arrowheads); the signal on L-D/V junctions (green arrowheads) is weak at the 1.5-fold stage and decreases during elongation. DLG-1 (purple) is a junction marker. Quantifications (A"-C") were made by measuring the membrane/cytoplasm ratio ("mb/cyto ratio") between PAR-3 staining at L-L or L-D/V junction for each stage (n=10 embryos 1,5-fold, 79 L-L / 137 L-D/V; n=10 embryos 2-fold, 80 L-L / 113 L-D/V; n=10 embryos 3-fold, 68 L-L / 113 L-D/V). The L-L / L-D/V ratio is shown in **D**. **E-J** PAR-3 is required for the recruitment of endogenous PAR-6::GFP (**E-G**) and GFP::PKC-3 (**H-J**) at L-L junctions. **G** and **J** correspond to quantifications of PAR-6 and PKC-3 recruitment, respectively, made by measuring the membrane/cytoplasm ratio ("mb/cyto ratio") at L-L junctions. **G**: n=22 control embryos, 66 L-L; n=22 *par-3(RNAi)* embryos, 66 L-L; **J**: n=30 control embryos, 90 L-L; n=23 *par-3(RNAi)* embryos, 69 L-L. **K-M** *par-3* depletion leads to actin misorientation (white arrowhead in L: n=15 embryos, 67 cells, compared to orange arrowheads in control, K: n=11 embryos, 34 cells) as confirmed by the associated quantification in **M**. The yellow box shows two cells (V2 and V3) (white arrowheads) where actin is oriented in the A/P axis leading to a cell elongation in the D/V axis; this phenotype was observed in 9/21 embryos (0/23 in control embryos). Actin cables in ventral and dorsal cells (blue arrowheads) are not affected. Quantification of actin orientation: vertical axis: D/V orientation; horizontal axis: A/P orientation. See also Figures S1 and S2. All embryos are imaged at the 2-fold stage except in A and C; anterior is to the left. Scale bars: 5 µm.
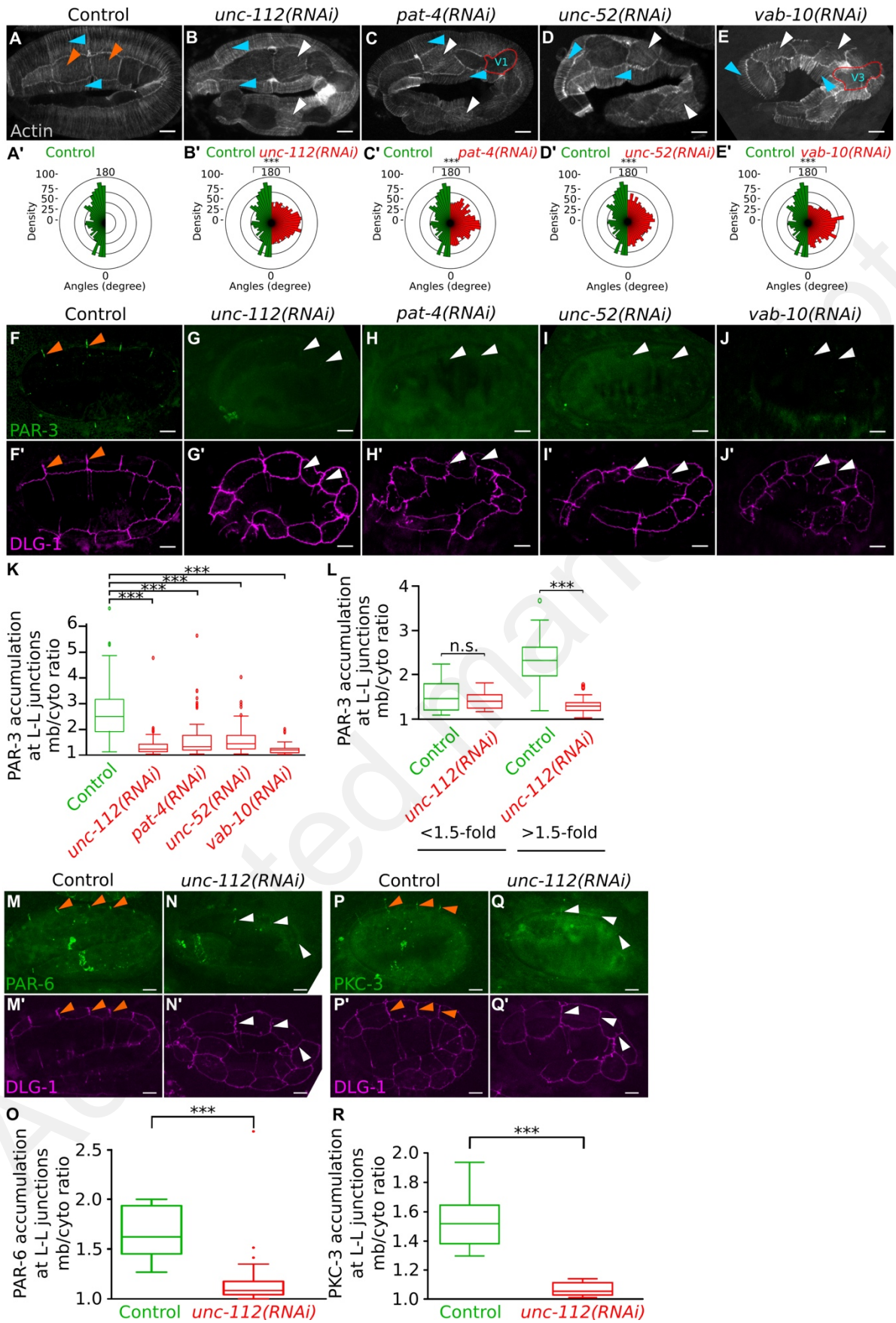
Figure 2: Muscles and molecular tendons are required for lateral epidermis planar polarity. A-E Actin organisation in lateral epidermal cells at the 2-fold stage; actin is disorganised upon *unc-112* (**B**; n=17 embryos, 61 cells), *pat-4* (**C**; n=19 embryos, 72 cells), *unc-52* (**D**; n=19 embryos, 61 cells) or *vab-10* (**E**; n=17 embryos, 39 cells) depletion. Orange arrowheads indicate proper actin polarisation in control cells (n=11 embryos, 34 cells) while white arrowheads indicate cells where actin is strongly disorganised; blue arrowheads indicate normal actin cable organisation in ventral and dorsal cells; V1 and V3 indicate cells which are elongated in the D/V axis. **A'-E'**: Quantification of actin orientation; vertical axis: D/V orientation; horizontal axis: A/P orientation. **F-J'** Depletion of *unc-112, pat-4, unc-52* or *vab-10* by RNAi leads to an absence of endogenous PAR-3::GFP at L-L junctions as depicted by white arrowheads compared to orange arrowheads in control. This absence of PAR-3 localisation at the plasma membrane has been quantified in **K** (n=20 control embryos, 112 L-L; n=29 *unc-112(RNAi)* embryos, 188 L-L; n=19 *pat-4(RNAi)* embryos, 132 L-L; n=21 *unc-52(RNAi)* embryos, 106 L-L; n=13 *vab-10(RNAi)* embryos, 82 L-L. **L** Quantification of PAR-3::GFP accumulation at L-L junctions in control and *unc-112* depleted embryos at early stages (left, n=21 control embryos, 25 *unc-112(RNAi)* embryos) and stages above the 1.5-fold stage (right, n=29 control embryos, 29 embryos *unc-112(RNAi)*); 3 L-L junctions are quantified for each embryo; see also Figure S2G which shows the same results as individual embryos with respect to the index elongation. **M-R** The depletion of *unc-112* also affects the localisation of endogenous PAR-6::GFP and GFP::PKC-3. In **O**: n=24 control embryos, 72 L-L; n=21 *unc-112(RNAi)* embryos, 63 L-L. In **R**, n=25 control embryos, 75 L-L; n=25 *unc-112(RNAi)* embryos, 75 L-L. See also Figure S2. All embryos were imaged and quantified at the 2-fold stage except in L; anterior is to the left. Scale bars: 5 µm.
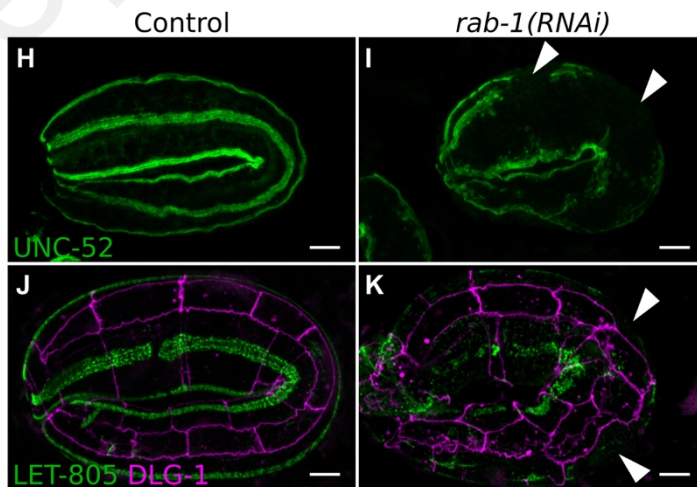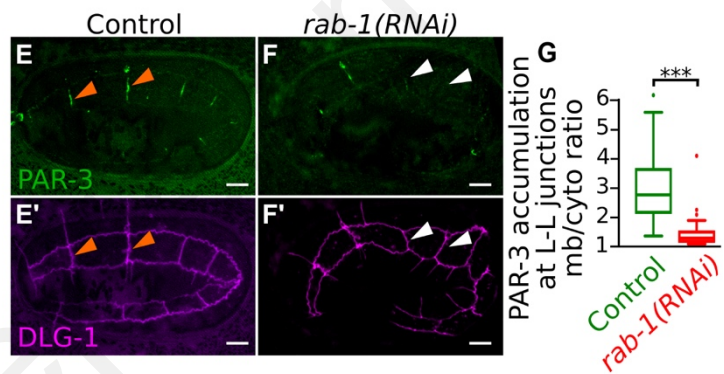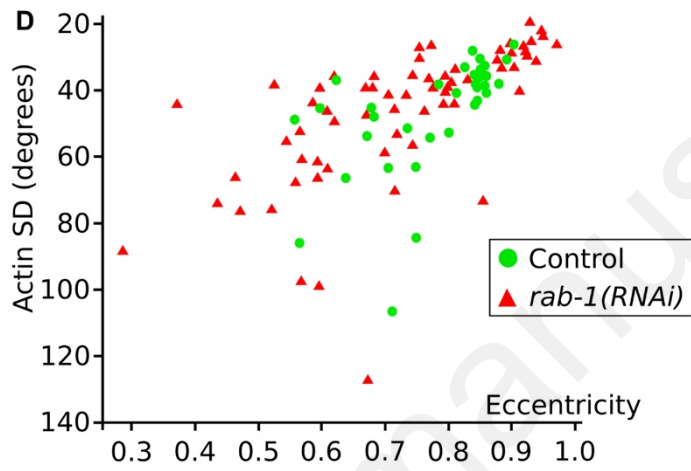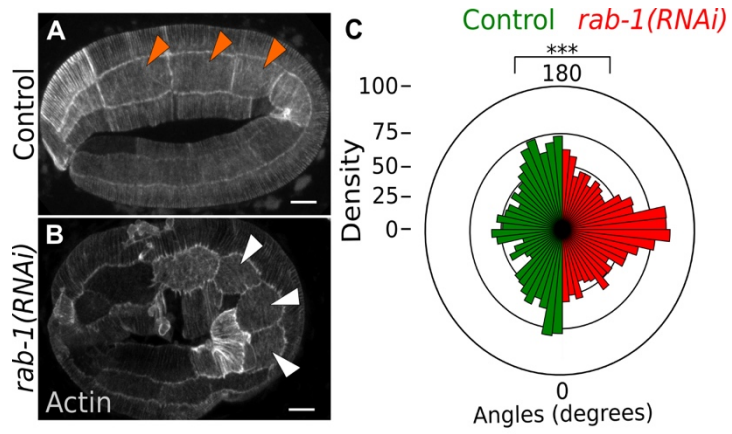
Figure 3: RAB-1 is required for planar polarity in the lateral epidermis through molecular tendon components localisation. **A-C** *rab-1* depletion leads to actin disorganisation in lateral epidermal cells at the 2-fold stage (n= 16 control embryos, 54 cells, orange arrowheads; n=16 *rab-1(RNAi)* embryos, 69 cells, white arrowheads where actin is mostly oriented in the A/P axis). Note that a high proportion of cells display an A/P orientation of actin (C). **D** Actin standard deviation and cell elongation (eccentricity) were plotted for control and *rab-1(RNAi)* embryos; each dot represents one cell (original data as in C); a Spearman test reveals a positive correlation ($p < 1.10^{-5}$) between the two parameters for both control and *rab-1(RNAi)* embryos. **E-G** Endogenous PAR-3::GFP localisation at L-L junctions observed in control embryos (orange arrowheads, n=26 embryos, 78 junctions) is lost under *rab-1* depletion (white arrowheads, n=12 embryos, 61 junctions). **G** corresponds to quantifications of PAR-3 accumulation at L-L junctions made by measuring the membrane/cytoplasm ratio ("mb/cyto ratio"). **H-K** *rab-1* depletion disrupts the localisation of endogenous UNC-52 as revealed by immunostaining (**H-I**; n=20 control embryos, n=15 *rab-1(RNAi)* embryos) and of endogenous LET-805::GFP using a CRISPR line (**J-K**; n=30 control embryos, n=24 *rab-1(RNAi)* embryos). White arrowheads indicate areas of interrupted staining; DLG-1 is a junction marker. See also Figure S3 and Table S1. All embryos are imaged at the 2-fold stage; anterior is to the left. Scale bars: 5 µm.

A Control

B *rab-1(RNAi)*

E-cad DLG-1

Ap Bl

C

E-cad L-DV/L-L ratio

n.s.

Control   *rab-1(RNAi)*

D

E-cad intensity (A.U.)

■ Control ■ *rab-1(RNAi)*

***   ***

L-L   L-D/V

E Control **F** *hmp-1(RNAi)*

PAR-3

E'   **F'**

DLG-1

G

PAR-3 accumulation at L-L junctions mb/cyto ratio

***

Control *hmp-1(RNAi)*

H Control   -3s   0   +3s +15s

D
A+P
V

I

D
A+P
V

J *rab-1(RNAi)*

D
A+P
V

K

Actin

D
A+P
V

L

(Af-Ao)/Ao

A/P cut D/V cut   A/P cut D/V cut

Control   *rab-1(RNAi)*
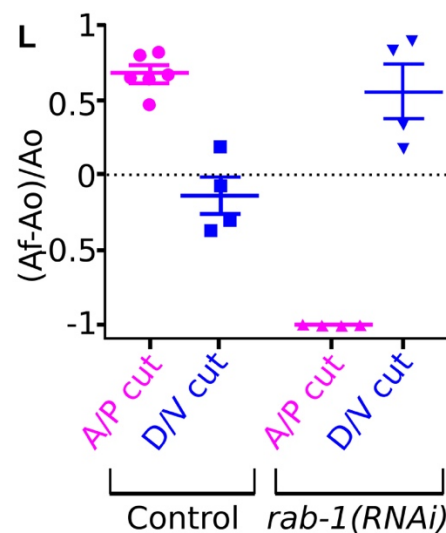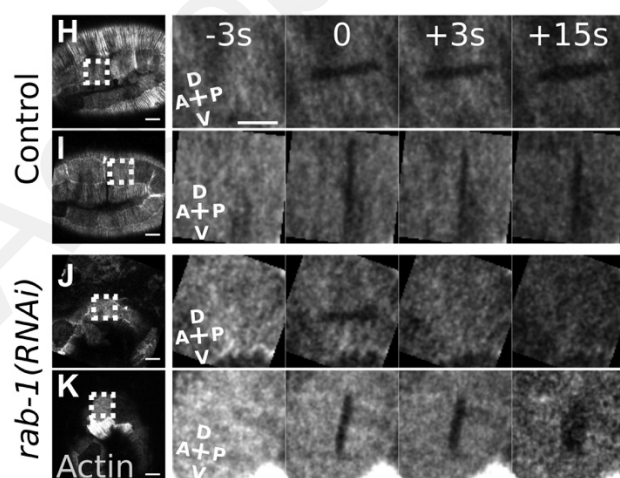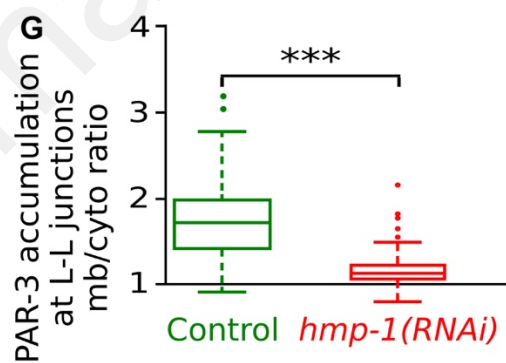
Figure 4: AJ function in signal transduction and role of actin planar polarity in tension orientation. A-D E-cadherin (in green) remains apical upon *rab-1* depletion (B, n=29 embryos) as in control embryos (A, n=18). Small insets correspond to Z-section represented by a white line in the associated picture: E-cadherin is localised above the junction marker DLG-1 (in purple). The quantification shows that the ratio of E-cadherin between L-D/V and L-L junctions remains intact under *rab-1* depletion (C). However, there is a slight decrease in E-cadherin overall accumulation at plasma membrane under *rab-1* depletion (D). **E-G** Endogenous PAR-3::GFP localisation at L-L junctions observed in control embryos (orange arrowheads, n=26 embryos, 78 junctions) is lost upon *hmp-1* depletion (white arrowheads, n=37 embryos, 111 junctions). **G** corresponds to quantifications of PAR-3 recruitment made by measuring the membrane/cytoplasm ratio ("mb/cyto ratio") at L-L junctions. **H-L** Laser nano-ablation experiments of the actin cytoskeleton in the lateral epidermis in control (**H-I**, actin oriented in the D/V axis) and *rab-1*-depleted (**J-K**, actin oriented in the A/P axis) embryos. Cuts were performed along the A/P axis (**H**, **J** in purple) or along the D/V axis (**I**, **K** in blue). These experiments have been quantified by measuring the relative expansion of the cut area over time; a value of 1 thus indicates an opening of the cut zone while 0 indicates no opening and -1 corresponds to closing (**L**; see STAR Methods for details). See also Figure S4. All embryos are imaged at the 2-fold stage; anterior is to the left. Scale bars: 5 µm.

STAR Methods

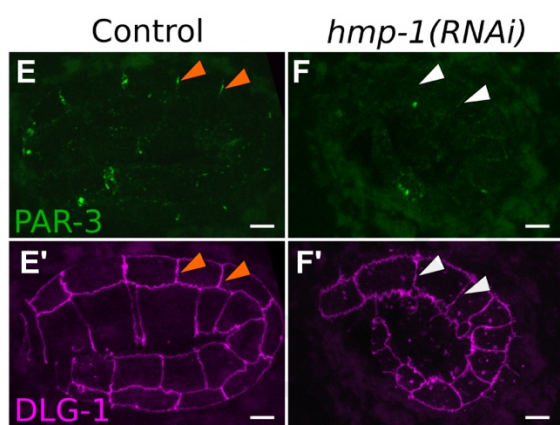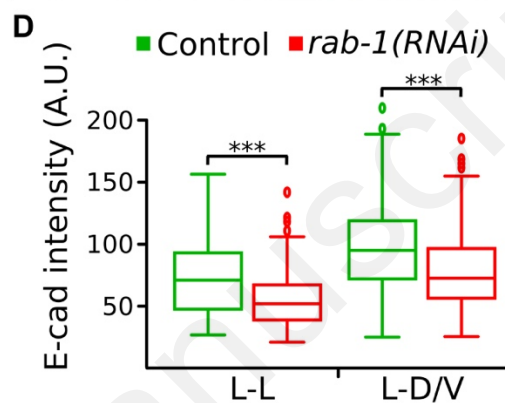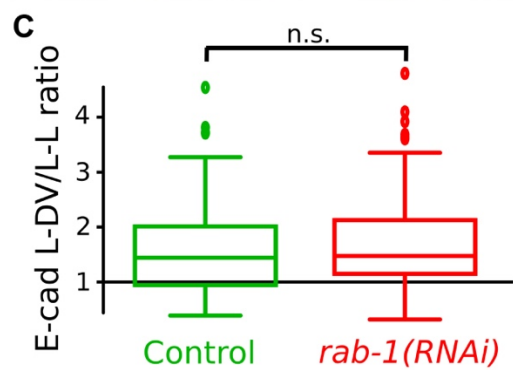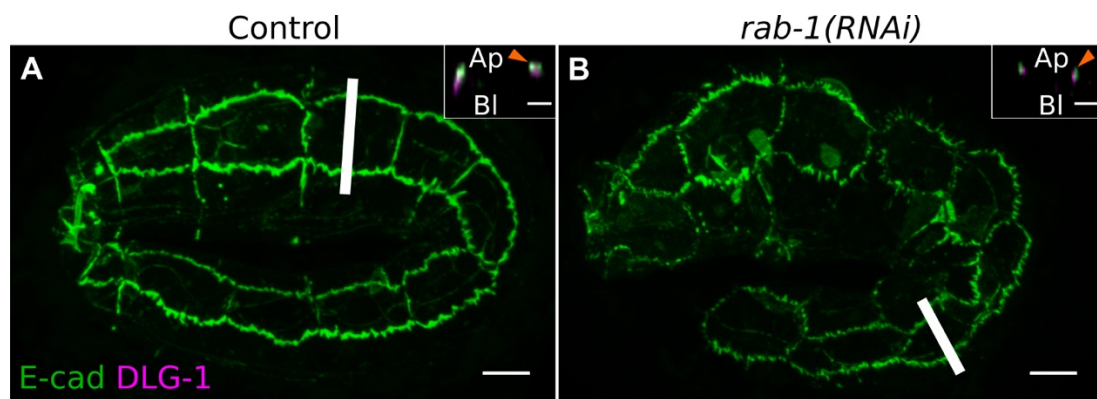## CONTACT FOR REAGENT AND RESOURCE SHARING

Further information and requests for resources and reagents should be directed to and will be fulfilled by the Lead Contact, Grégoire Michaux (gmichaux@univ-rennes1.fr).

EXPERIMENTAL MODEL AND SUBJECT DETAILS

C. elegans and *C. briggsae* strains were used in this study. All analysed animals were hermaphrodites and at the embryonic stage at the time of observations. Figure legends indicate the precise embryonic stage for each experiment.

- Health/immune status : not applicable
- Subjects were never involved in previous procedures
- All embryos were drug and test naïve
- The genotypes of the strains used in this study are detailed in the Key Ressource Table.
- Species/strain of experimental models: all embryos were derived from the *C. elegans* N2 Bristol isolate. The *C. briggsae* strain is derived from AF16 Indian isolate.
- Husbandry conditions: *C. elegans* and *C. briggsae* strains were maintained and crossed on NGM plates seeded with *E. coli* OP50 at 20°C.

METHOD DETAILS

Overview
All experiments were replicated at least three times except for the *par-6* depletion wich was replicated two times. No strategy was used for randomization or stratification; no blinding was used, and sample-size were not estimated. No data were excluded during quantifications.

Plasmid construction and strains
The *C. briggsae* version of *rab-1* (called *Cbr-rab-1*) was amplified from the ANA020 strain [45] by PCR with the Phusion Master Mix then cloned in the Gateway pDONR p221 with the Gateway BP Clonase Enzyme Mix. The construct was injected at 5 ng/µL together with the *rol-6(su1006)* marker at 100 ng/µL in the *C. elegans* N2 strain.

RNAi
Embryonic RNAi was performed by feeding using the Ahringer-Source BioScience library [46-48]; RNAi was induced in young adults and the phenotypes observed in the next generation (F1). L4440 corresponds to the standard control RNAi feeding strain. For some genes (e.g. *par-3, par-6*) the duration of the RNAi treatment was adapted (<24 h) to observe elongation phenotypes while avoiding earlier developmental phenotypes usually associated with these genes; *rab-1(RNAi)* was induced for about 20 h to avoid the sterility triggered in

the parental generation. All embryos observed and used for quantifications were 7-10 h old, corresponding to 1.5- to 3-fold embryos in a WT strain; as a control we checked that there was not expression of the *myo-2p::GFP* transgene which is expressed from the 3-fold stage and present in the FL311 strain used to localize ABD::GFP. RNAi efficiency was checked by observing the induction of a developmental arrest whenever such a phenotype was expected based on previous reports. To test the specificity of the *rab-1(RNAi)* we scored the embryonic lethality observed following *Cel-rab-1(RNAi)* in an N2 strain and in a strain expressing *Cbr-rab-1* as presented in Figure S3A-B.

Immunostaining

Fixation of embryos was performed using the freeze-crack methanol protocol [49]. Briefly, embryos were squeezed for 2 min before being frozen in liquid nitrogen, fixed in methanol for 20 min and washed in PBS. After a blocking step in PBS-Tween 0.2% supplemented with 1% BSA for 20 min, embryos were incubated with the primary antibody at 4°C overnight then with the secondary antibody at 1 h at 37°C in a wet chamber. Embryos were finally mounted in 10 µL Mowiol. We used the anti-UNC-52 MH2 (1/50) monoclonal antibody from DSHB (University of Iowa, USA). Alexa Fluor 488 antibody (ThermoFisher) was used as secondary antibody. All antibodies were diluted in PBS-Tween 0.2%.

Electron microscopy

To prepare samples for electron microscopy experiments embryos were fixed by high pressure freezing followed by freeze substitution, flat embedding to allow antero-posterior orientation and sectioning [48]. Control (n=3) and *rab-1(RNAi)* (n=4) embryos were observed. Each embryo was sectioned every 5-7μm to ensure that different cells were observed in different 5-7μm segments; 3 segments were examined for each embryo. The pictures in Figure S4L-M are representative of all the sections observed. Observations were performed on a Jeol JEM1400 equipped with a Gatan Orius SC1000 camera.

Confocal microscopy

Confocal observations were performed on 1.5-, 2-, and 3-fold stage embryos. From the 1.5-fold stage embryos start moving due to muscle contractions; from the 1.8-fold stage they move too rapidly for imaging and these movements completely prevent obtaining movies of the progressive planar polarization of the PAR module and of actin. To image these embryos, we added bacteria to the mounting medium M9. This treatment results in progressive hypoxia leading to muscle inactivity and immobilisation. Embryos were then imaged using Leica (Wetzlar, Germany) SPE, SP5 or SP8 confocals equipped with 63X/1.4 HCX PL APO objectives (LAS AF software). The SP5 and SP8 confocals are equipped with hybrid detectors which were used to image the low signals generated by the genome-edited strains expressing PAR-3::GFP, PAR-6::GFP and GFP::PKC-3 at the endogenous level. They were also used to image ABD::GFP at the highest possible resolution with a low background. All images were examined using ImageJ 1.43 or Fiji 1.0 and assembled using the Inkscape software. No image

manipulation was performed except adjusting contrast and brightness in an homogenous way throughout the picture.

FRAP experiments
FRAP experiments were performed on 1.5-fold stage embryos just before the onset of muscle contractions. We used an inverted Nikon Ti-E microscope equipped with a Spinning-disk CSU-X1 and a single-point scanning head to allow laser microirradiation. Embryos were imaged with a 63X/1.4 PLAN APO objective and fluorescence was collected with an sCMOS ORCA Flash 4.0 camera. The FRAP was performed on a whole junction with 100% laser power, 50 iterations and a line thickness of 2, in the iLAS software in Metamorph. Post-FRAP images were acquired every 10 seconds.

Laser nano-ablations
Laser nano-ablation experiments were performed on 2-fold stage embryos. Because at that stage embryos move too rapidly for imaging we prevented movements by adding bacteria to the mounting medium M9. This treatment results in progressive hypoxia leading to muscle inactivity and immobilization. To perform ablations, we selected embryos which had just stopped moving and used an inverted Leica SP5 microscope equipped with a Pulsed laser Mai Tai HP Ti. Embryos were imaged with a 63X/1.4 HCX PL APO objective. Laser nano-ablations were performed at 800 nm with a single iteration. Images were acquired every 1.27 seconds.

QUANTIFICATION AND STATISTICAL ANALYSIS

Overview
The percentage of embryos displaying a phenotype was obtained either by direct observation or after quantification. All quantifications were performed on images acquired in independent experiments (no embryo was measured repeatedly). Gaussian distribution and similar variances were tested before performing statistical analysis.

Fluorescence intensity measurements
Quantifications were performed using ImageJ 1.43 or Fiji 1.0 along lines (length 5-10 μm, width 0.3 μm) over the membrane and cytoplasmic parts of at least three cells for each embryo. The membrane quantification was normalised to the cytoplasmic background; a ratio of 1 therefore indicates no specific membrane localisation. In Figure 4D and Figure S4H we measured intensity along the membranes and plotted these numbers directly, without normalisation to the cytoplasm.

Actin orientation in lateral epidermal cells
Actin orientation was measured in Matlab using custom-routines [50]. Briefly local directors representing actin alignment were determined as follows for each cell: a cell was properly

oriented and broken in small overlapping windows of 2.6*2.6 μm and the 2D FFT of each filtered window was calculated, giving a range of angles whose values are given compared to the dorso-ventral axis. Each count is the dominant angle for a particular 2.6 µm square analysis window, and each count is plotted. Representative cell with actin local directors are shown in Figure S1. The data are shown on plots as a percentage of counts in a given angle class / all counts and there is one class for every 6° angle (30 classes to cover 180°) for all the plots.

FRAP quantifications
Quantifications were made manually in Image J by measuring the mean intensity of the bleached junction after background subtraction.

Actin organisation and cell elongation axis
We exploited a Matlab script written by Gomez et al [51]. We used it to recognise and analyse the cytoskeleton organisation in 8-bit images of embryonic lateral cells. Inputs files are two subfolders that contain an image of a cell border, an image of the embryo and the other contains the cytoskeleton projection inside a given cell. The script recognises the cytoskeleton and the cell borders using the generated mask. The script fits the cell as an ellipse and calculate the eccentricity and the standard deviation SD. SD measures actin alignment with respect to the major axis of the ellipse. The eccentricity calculated using Matlab is defined as the ratio of the distance between the foci of the ellipse and its major axis length. If the eccentricity is 0, the ellipse is a circle and if it is equal to 1 the ellipse is equivalent to a segment. To do so, the signal of each pixel is extracted using the cell mask and the gradient of the signal is calculated using a Sobel filter (5x5). The magnitude M depends on the signal gradient along x and y and is used to quantify the direction of its pixel and its changes. We plotted the eccentricity of each cell (elongation axis) as a function of the standard deviation of the actin signal in the same cell in order to obtain the correlation between the cell elongation axis and actin orientation

Laser nano-ablation quantifications
For quantifications, the cut zone was manually tracked over time in ImageJ and the relative expansion was calculated as follows: $(l_{15} - l_0)/l_0$ where l is the small axis of the cut zone; 0 and 15 correspond to the first picture after the cut and the picture after 15 seconds, respectively. A value of 1 thus indicates an opening due to relaxation, while 0 indicates no relaxation and -1 corresponds to a closing by contraction and/or compression; compression could be passive, possibly due to pushing forces exerted by the dorsal and ventral epidermis and contraction could be due to actin dynamics within lateral cells.

Statistical analysis
To determine whether the data met assumptions of the statistical approaches used we first analysed the data distribution and the variances. Parametric T-tests were used when samples had a Gaussian distribution and similar variances. Other cases were treated using non-

parametric Wilcoxon tests. Actin distribution was treated using a X^2 test. A Spearman correlation test was used to determine the correlation between actin standard deviation and cell eccentricity. Significance is indicated as follows: * $p<0.05$, ** $p<0.01$, *** $p<0.001$. Quantification results are shown as box plots: centre line: median; box: first and third quartiles; whiskers: 10th and 90th percentiles. In all Figure legends, n refers to the number of different embryos analysed for a particular experiment. These legends also clearly indicate the number of junctions/cells analysed for each experiment.
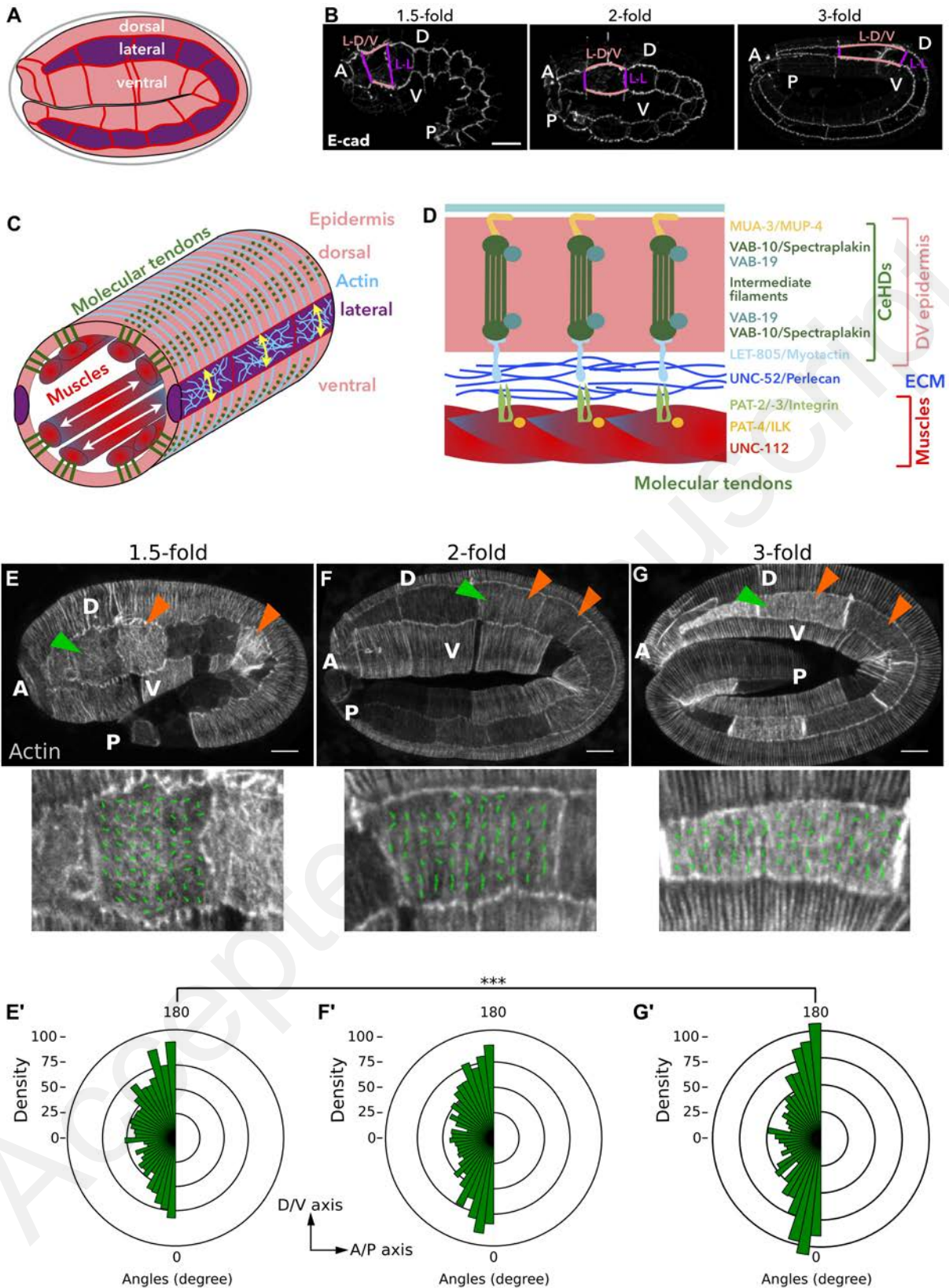
Figure S1: Embryo anatomy; actin planar polarisation – related to Figure 1. A-D Schematic representation of *C. elegans* anatomy and junctional organisation during morphogenesis. **A** The epidermis is divided into three parts: the ventral and the dorsal epidermis (pink) which share the same developmental program, and two rows of ten cells, one on each side of the embryo, the lateral epidermis (purple). **B** Lateral view of *C. elegans*

embryos during elongation showing the apical membrane of epidermal cells in the plane of the figure; note that all pictures will display the same orientation in all figures except for TEM pictures. The elongation of the embryo reflects the elongation of the cells from the lateral epidermis. These cells exhibit a planar polarity: junctions between lateral cells (L-L junctions, purple) shrink during elongation while the junctions between dorsal or ventral cells and lateral cells (L-D/V junctions, orange) elongate in the axis of embryonic elongation. **C** The embryo can be assimilated to a tube surrounded by the epidermis. Muscles lay beneath the basolateral membrane of the dorsal and ventral epidermis, linked to the apical side by molecular tendons (C-D); muscles contract in the A/P axis (white double arrows) and in the lateral epidermis actomyosin contractions are organised in the D/V axis (yellow double arrows). **D** Molecular tendons link the muscles to the dorsal and ventral epidermis through the extracellular matrix (ECM) and the whole dorso-ventral epidermis thickness to the apical surface and the apical ECM. CeHDs are mainly composed by apical transmembrane receptors (MUA-3, MUP-4), intermediate filaments, linker proteins (VAB-19, VAB-10) and a basolateral receptor (LET-805). The basal ECM (UNC-52) is in turn linked to muscles through the action of integrins which require PAT-4 and UNC-112 for their proper localisation. **E-G** Actin orients along the dorso-ventral axis during elongation, from the 1.5-fold stage, where it exhibits a partial orientation along the D/V axis (n=19 embryos, 51 cells) to the 2-fold (n=18 embryos, 57 cells) and the 3-fold stages (n=15 embryos, 48 cells) where actin is strongly oriented along the D/V axis (orange arrowheads); pictures in the second row are enlarged individual cells (green arrowheads) of the embryo above, with the A/P axis aligned along an horizontal line, showing individual actin local directors as calculated. **E'-G'** Actin orientation in epidermal cells has been quantified for each cell as described [S1]. Graphs represent the distribution of angles compared to the D/V axis: vertical axis: D/V orientation; horizontal axis: A/P orientation. In all panels, anterior is to the left. Scale bars: 5 µm.
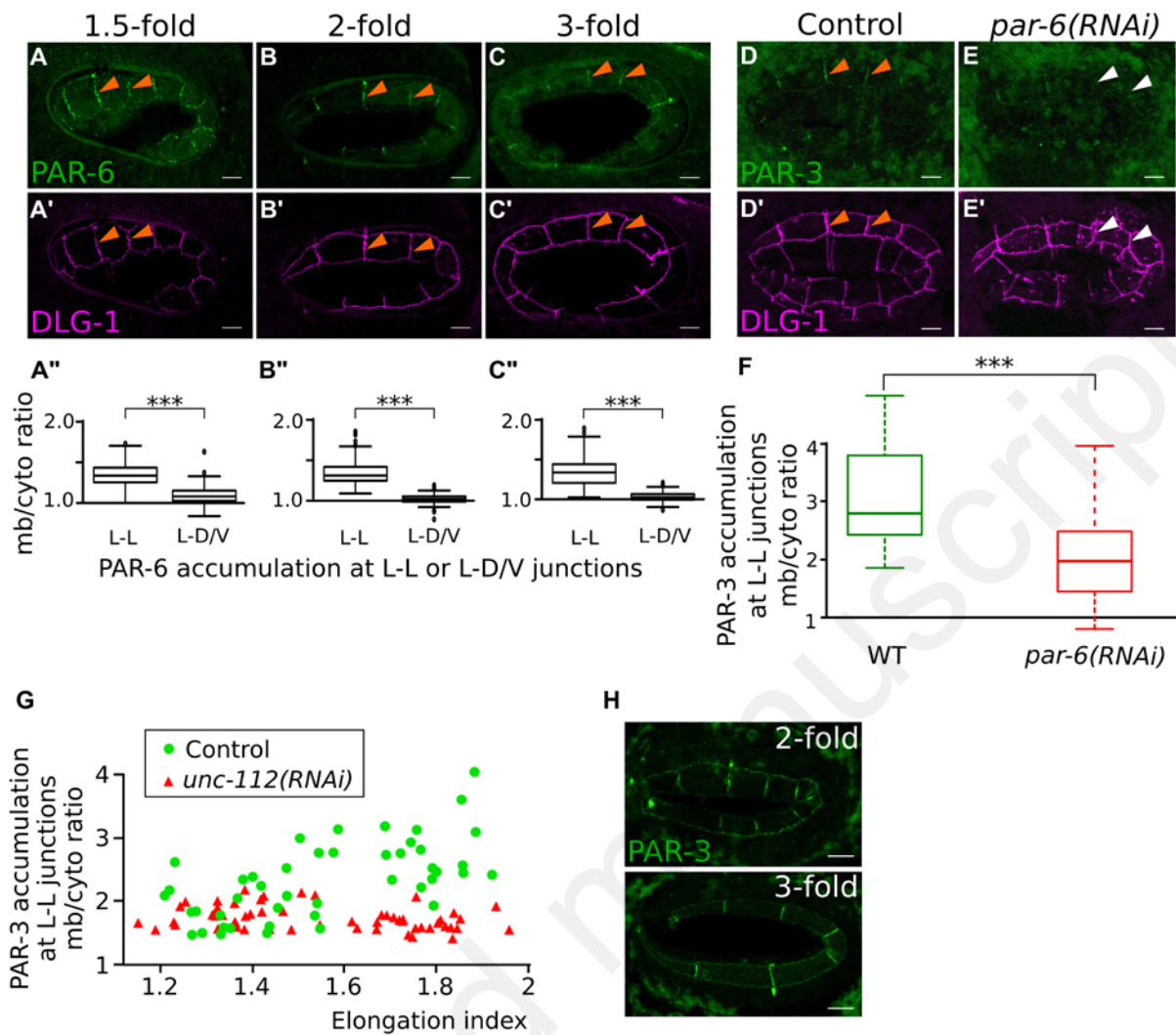
Figure S2: PAR planar polarity in the lateral epidermis – related to Figure 1. A-C"
Endogenous PAR-6::GFP accumulates at the L-L junctions (orange arrowheads) during
elongation in control embryos as revealed by the associated quantifications made on L-L and
L-D/V junctions (ratio of membrane/cytoplasm localisation; n=10 1.5-fold stage embryos 74
L-L, 121 L-D/V; n=10 2-fold stage embryos, 78 L-L, 120 L-D/V; n=10 3-fold stage embryos,
71 L-L, 106 L-D/V). **D-F** The depletion of *par-6* by RNAi prevents PAR-3 recruitment at L-L
junctions (white arrowheads), compared to control embryos where PAR-3 accumulates at L-L
junctions (orange arrowheads); n=15 control embryos; n=8/11 *par-6(RNAi)* embryos. **G**
Quantification of PAR-3::GFP on L-L junctions in control and *unc-112* depleted embryos
during elongation; the index is based on the elongation of each embryo between 1.2- and 2-
fold stage (n=50 control embryos, 150 L-L; n=54 *unc-112(RNAi)* embryos, 162 L-L); see also
Figure 2L which shows the same results split in two groups, before and after 1.5-fold stage. **H**
Representative images of PAR-3::GFP localisation at 2-fold and 3-fold stages obtained with
another strain [S2]; PAR-3 was planar polarised in all observed embryos (n>10). All embryos
are imaged at the 2-fold stage except in A-A', C-C' and H; anterior is to the left except in C-
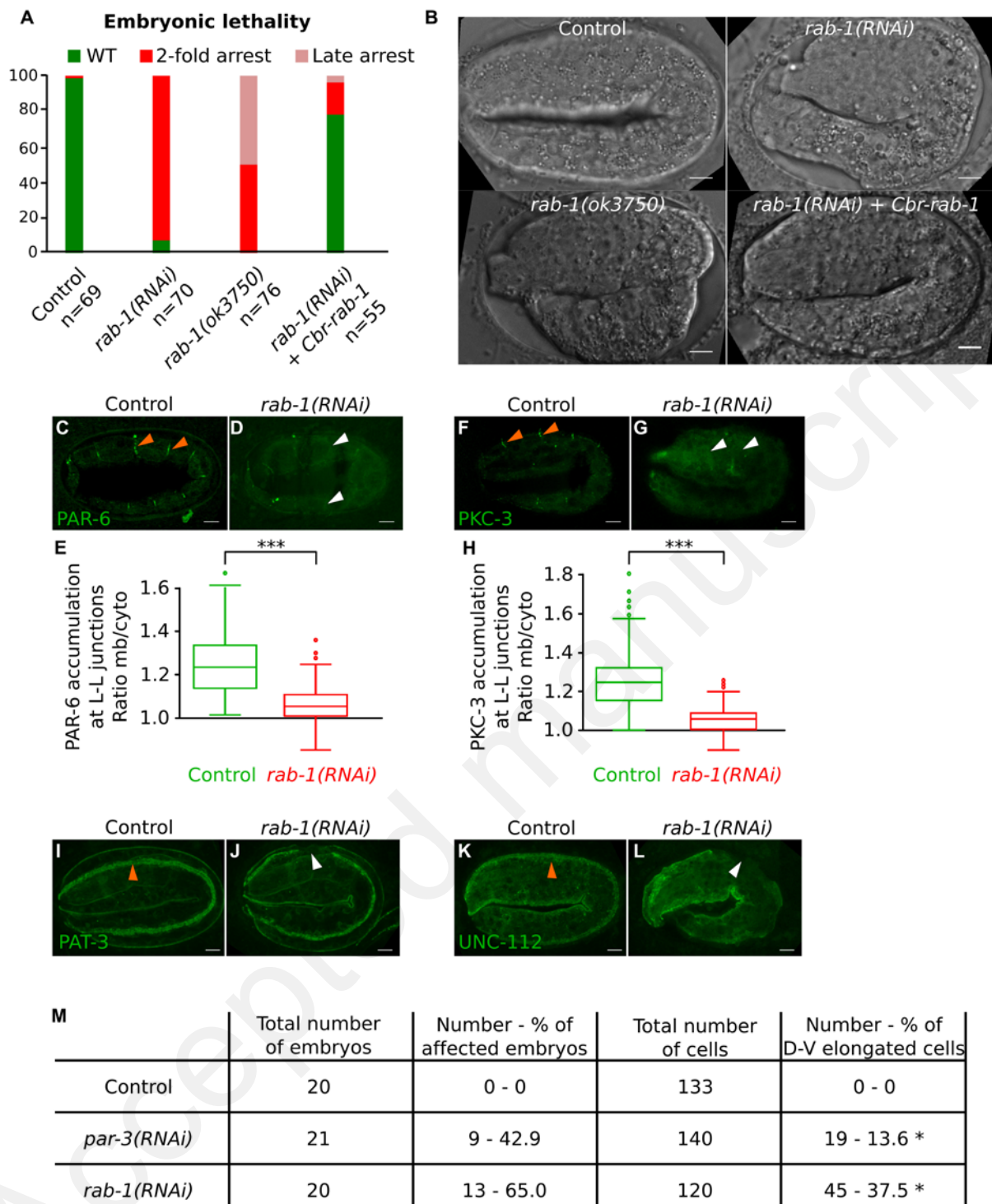C'. Scale bars: 5 µm.

M	Total number of embryos	Number - % of affected embryos	Total number of cells	Number - % of D-V elongated cells
Control	20	0 - 0	133	0 - 0
par-3(RNAi)	21	9 - 42.9	140	19 - 13.6 *
rab-1(RNAi)	20	13 - 65.0	120	45 - 37.5 *

Figure S3: *rab-1* **depletion induces a 2-fold arrest and loss of PAR-6 and PKC-3 – related to Figure 3. A-B** The depletion of *rab-1* by RNAi induces a very robust 2-fold arrest. The expression of an RNAi-resistant version of *rab-1* from *C. briggsae* almost fully rescues the lethality induced by *rab-1* depletion by RNAi and the deletion allele *rab-1(ok3750)* phenocopies *rab-1(RNAi)*. **C-H** The depletion of *rab-1* affects the localisation of endogenous PAR-6::GFP and GFP::PKC-3; orange arrowheads show normal staining, white arrowheads indicate absence of staining. In E: n=21 control embryos, 149 junctions; n=25 *rab-1(RNAi)* embryos,186 junctions. In H : n=20 control embryos, 128 junctions; n=23 *rab-1(RNAi)* embryos, 144 junctions. **I-L** *rab-1* depletion disrupts the localisation of PAT-3 ::GFP

(n=26/27 unaffected control embryos; n=16/21 affected *rab-1(RNAi)* embryos) and UNC-112 ::GFP (n=33/36 unaffected control embryos; n=42/49 affected *rab-1(RNAi)* embryos). Orange arrowheads show normal staining, white arrowheads indicate areas of interrupted staining. **M** Number and percentage of embryos and cells displaying cells with a D/V elongation axis instead of the normal A/P elongation axis observed in control embryos at the 2-fold stage. *rab-1(RNAi)* embryos display a more penetrant phenotype compare to *par-3(RNAi)* embryos. * All cells elongated in the D/V axis display a strict A/P organisation of actin. All embryos are imaged at the 2-fold stage. Scale bars: 5 µm.
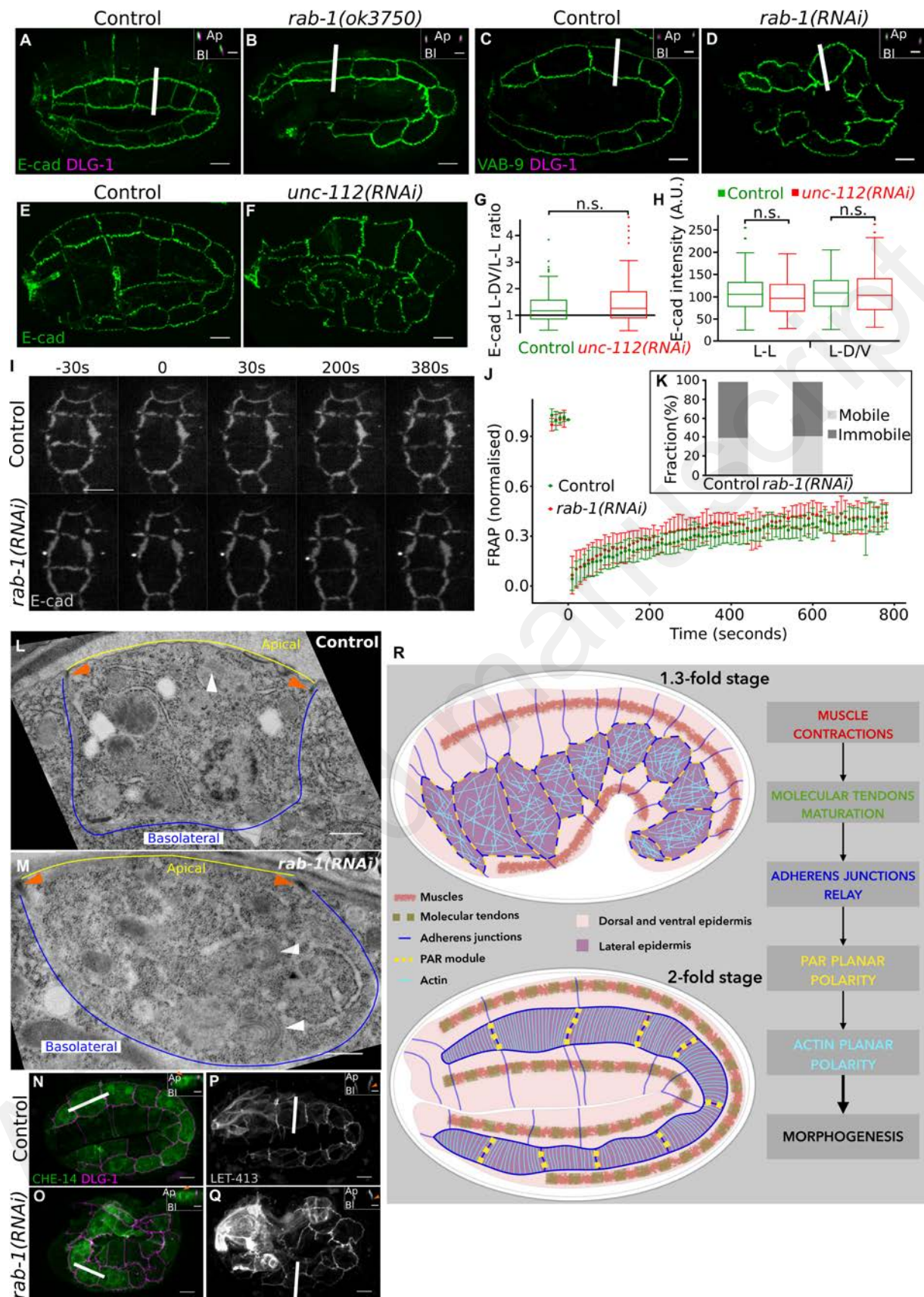
Figure S4. Junction integrity and apico-basal polarity are not affected upon CeHDs depletion – related to Figure 4. A-B E-cad (green) remains apical in *rab-1(ok3750)* mutant embryos (B, n=28) as in control embryos (A, n=18). Small insets correspond to Z-section

represented by a white line in the associated picture: E-cad is localised above the junction marker DLG-1 (purple). **C-D** VAB-9, another component of AJs [S3], also remains apical above DLG-1 upon *rab-1* depletion (n=13 embryos) as in control (n=14 embryos). **E-H** E-cad localisation is not affected upon *unc-112* depletion: the weak planar polarity (G) and the signal intensity at the L-L and L-D/V junctions (H) are conserved. **I-K** FRAP experiments performed in 1.5-fold stage embryos show that E-cad dynamics is not affected in the absence of RAB-1 (n=7 junctions for control, n=8 for RNAi embryos), as depicted on the recovery curves (J; error bars indicate standard deviation) and the percentages of mobile and immobile fractions (K). **L-M** Transmission electron microscopy (TEM) reveals that the electron-dense region corresponding to the junctions (orange arrowhead) is still properly localised upon *rab-1* depletion in these cross-sections of lateral cells; however Golgi cisternae (white arrowhead) were systematically curled in *rab-1(RNAi)* embryos (n≥3 embryos for each condition). **N-Q** Apico-basal polarity is not affected upon *rab-1* depletion. CHE-14 remains apical (**N-O**; n=16 and n=20, respectively), while LET-413 remains lateral (**P-Q**; n=18 and n=29, respectively); orange arrowheads indicate proper localisation, apical for CHE-14 or at the lateral membrane for LET-413. All embryos are imaged at the 2-fold stage including for the TEM pictures, except in I (1.5-fold) Ap: apical; Bl: basolateral. Scale bars: 5 µm, except for small insets: 2 µm, and for L-M: 0.5 µm. **R** Working model. Before the 1.5-fold stage actin is disorganised and actomyosin contractions in lateral cells drive elongation; the PAR module starts to be recruited in an unpolarised manner. From the 1.5-fold stage muscle contractions promote the assembly and the stabilisation of CeHDs [S4] to enable force transmission between muscles and the dorsal and ventral epidermis through molecular tendons during morphogenesis. This force is then relayed by adherens junctions from the dorsal and ventral epidermis to the lateral epidermis. This leads to bipolar PAR planar polarity and ultimately actin orientation along the dorso-ventral axis, a prerequisite to properly control cell shape changes and therefore elongation along the antero-posterior axis.

Gene list	Sequence	Short description
agef-1	Y6B3A.1	Putative ARF guanine nucleotide exchange factor orthologous to human ARFGEF1 and ARFGEF2
apa-2	T20B5.1	Ortholog of the alpha subunit of adaptor protein complex 2
apm-2	R160.1	Ortholog of the mu2 subunit of adaptor protein complex 2
aps-1	F29G9.3	Ortholog of the sigma subunit of adaptor protein complex 1
arf-1.2	B0336.2	ADP-ribosylation factor homolog
atn-1	W04D2.1	Alpha-actinin homolog
cdh-4	F25F2.2	Fat-like cadherin homolog
ced-5	C02F4.1	Homolog of the human protein DOCK180
chc-1	T20G5.1	*C. elegans* clathrin heavy chain ortholog
cogc-3	Y71F9AM.4	Ortholog of mammalian COG-3/Sec34, a subunit of lobe A of the conserved oligomeric Golgi complex (COGC)
cogc-4	Y51H7C.6	Ortholog of mammalian COG-4, a subunit of lobe A of the conserved oligomeric Golgi complex (COGC)
copb-1	Y25C1A.5	Beta subunit of the coatomer (COPI) complex
copb-2	F38E11.5	Beta' (beta-prime) subunit of the coatomer (COPI) complex
/	T14G10.5	Gamma subunit of the coatomer (COPI) complex
copz-1	F59E10.3	Zeta subunit of the coatomer (COPI) complex
cul-1	D2045.6	Cullin, orthologous to Cdc53/Cul1 in S. cerevisiae and CUL-1 in humans
dnc-1	ZK593.5	*C. elegans* ortholog of the dynactin complex subunit p150/GLUED/DCTN1
fln-1	Y66H1B.2	Filamin ortholog
gbf-1	C24H11.7	Ortholog of human GBF1 (golgi brefeldin A resistant guanine nucleotide exchange factor 1)
/	F33G12.5	Ortholog of human GOLGA6A (golgin A6 family member A)
golg-4	F59A2.6	Ortholog of human ppl (periplakin) and EVPL (envoplakin)
hum-2	F36D4.3	Class V unconventional myosin similar to human MYO5A, MYO5B and MYO5C
hum-5	T02C12.1	Ortholog of human MYO1D (myosin ID) and MYO1G (myosin IG)
magi-1	K01A6.2	Multi PDZ-domain containing tight junction-associated protein: MAGIs are members of vertebrate membrane associated guanylate-kinase (MAGUK) family
mdt-9	Y62E10A.11	Ortholog of human RABIF (RAB interacting factor)
mec-7	ZK154.3	Beta-tubulin
nmy-2	F20G4.3	Non-muscle myosin II
ocrl-1	C16C2.3	Inositol-1,4,5-triphosphate 5-phosphatase homolog that is homologous to human OCRL
rab-1	C39F7.4	Ortholog of the small Ras-like GTPase Rab1
rab-2	F53F10.4	Small GTPase homologous to the Rab GTPases that function in endocytosis, membrane fusion, and vesicular trafficking events
rab-35	Y47D3A.25	Small, monomeric Rab GTPase that is most closely related to the human and *Drosophila* Rab35 GTPases
rab-5	F26H9.6	Rab5 GTPase ortholog
rab-6.1	F59B2.7	Small, monomeric Rab GTPase that is most closely related to the *Drosophila* and mammalian Rab6 GTPases
rabn-5	F01F1.4	Ortholog of Rabaptin-5, a Rab5 effector protein
rabx-5	Y39A1A.5	Protein containing a zinc-finger domain and a Vps9 domain that is the *C. elegans* ortholog of the Rabex-5 Rab5 guanine-nucleotide exchange factor
rack-1	K04D7.1	Seven-WD repeat-containing protein that is the *C. elegans* ortholog of vertebrate Receptor for Activated C Kinase
ran-1	K01G5.4	Ran GTPase ortholog
sar-1	ZK180.4	Ortholog of human SAR1A (secretion associated Ras related GTPase 1A) and SAR1B (secretion associated Ras related GTPase 1B)
sec-23	Y113G7A.3	Component of COPII (coat protein complex II)-coated vesicles orthologous to Saccharomyces cerevisiae Sec23p
sec-24.1	F12F6.6	Encodes one of two *C. elegans* Sec24 homologs
sec-31	T01G1.3	Ortholog of human SEC31A (SEC31 A, COPII coat complex component) and SEC31B (SEC31 B, COPII coat complex component)
sma-1	R31.1	Beta-H spectrin

spc-1	K10B3.10	Alpha spectrin ortholog
sql-1	Y111B2A.4	Ortholog of human TRIP11 (thyroid hormone receptor interactor 11)
syx-5	F55A11.2	Ortholog of human STX5 (syntaxin 5)
/	T04C9.1	Orthologous to the human gene GRAF PROTEIN
tba-1	F26E4.8	One of nine *C. elegans* alpha-tubulins
tba-2	C47B2.3	One of nine *C. elegans* alpha-tubulins
tba-4	F44F4.11	One of nine *C. elegans* alpha-tubulins
tba-9	F40F4.5	One of nine *C. elegans* alpha-tubulins
tbb-2	C36E8.5	Homolog of mammalian beta-tubulin (TUBB)
tbcd-1	F16D3.4	Putative beta-tubulin folding cofactor D
tln-1	Y71G12B.11	Ortholog of human TLN2 (talin 2) and TLN1 (talin 1)
unc-70	K11C4.3	Two isoforms of a beta-spectrin ortholog
uso-1	K09B11.9	Ortholog of the Uso1/p115 vesicle tethering protein that in yeast has been shown to function in endoplasmic reticulum-to-Golgi transport
vps-35	F59G1.3	Ortholog of human Vps35 (VPS35, retromer complex component)

Table S1: List of candidate genes targeted in the screen for PAR-3 localisation and actin organisation – related to Figure 3. These genes were selected based on their role in membrane traffic, cytoskeleton regulation or developmental phenotype. Except for *rab-1*, none of these depletions induced actin disorganisation or PAR-3 loss at L-L junctions at the 2-fold stage.

SUPPLEMENTAL REFERENCES

S1.   Cetera, M., Ramirez-San Juan, G.R., Oakes, P.W., Lewellyn, L., Fairchild, M.J., Tanentzapf, G., Gardel, M.L., and Horne-Badovinac, S. (2014). Epithelial rotation promotes the global alignment of contractile actin bundles during Drosophila egg chamber elongation. Nat Commun *5*, 5511.

S2.   Achilleos, A., Wehman, A.M., and Nance, J. (2010). PAR-3 mediates the initial clustering and apical localization of junction and polarity proteins during C. elegans intestinal epithelial cell polarization. Development *137*, 1833-1842.

S3.   Simske, J.S., Koppen, M., Sims, P., Hodgkin, J., Yonkof, A., and Hardin, J. (2003). The cell junction protein VAB-9 regulates adhesion and epidermal morphology in C. elegans. Nature cell biology *5*, 619-625.

S4.   Zhang, H., Landmann, F., Zahreddine, H., Rodriguez, D., Koch, M., and Labouesse, M. (2011). A tension-induced mechanotransduction pathway promotes epithelial morphogenesis. Nature *471*, 99-103.